Biomedical Optics EXPRESS

Imaging cytosolic translocation of *Mycobacteria* with two-photon fluorescence resonance energy transfer microscopy

Yassel Acosta,[1,4] Qi Zhang,[2,4] Arifur Rahaman,[1] Hugues Ouellet,[2] Chuan Xiao,[3] Jianjun Sun[2,5] and Chunqiang Li[1,*]

[1]*Department of Physics, The University of Texas at El Paso, 500 W. University Ave., El Paso, Texas 79968, USA*
[2]*Department of Biological Sciences, The University of Texas at El Paso, 500 W. University Ave., El Paso, Texas 79968, USA*
[3]*Department of Chemistry, The University of Texas at El Paso, 500 W. University Ave., El Paso, Texas 79968, USA*
[4]*These authors contribute equally*
[5]*jsun@utep.edu*
[*]*cli@utep.edu*

Abstract: Transition from latency to active tuberculosis requires *Mycobacterium tuberculosis* (*Mtb*) to penetrate the phagosomal membrane and translocate to the cytosol of the host macrophage. Quantitative two-photon fluorescence resonance energy transfer (FRET) microscopy is developed to measure cytosolic translocation using *Mycobacterium marinum* (*Mm*) as a model organism for *Mtb*. Macrophages were infected with *Mm* or non-pathogenic *Mycobacterium smegmatis* (*Ms*) as a control, then loaded with a FRET substrate. Once translocation occurs, *mycobacterium*-bearing β-lactamase cleaves the substrate, resulting in decrease of FRET signal. Quantification of this FRET signal change revealed that *Mm*, but not *Ms*, is capable of translocating to the cytosol.

OCIS codes: (170.2520) Fluorescence microscopy; (170.1530) Cell analysis.

References and links

1. P. J. Dolin, M. C. Raviglione, and A. Kochi, "Global tuberculosis incidence and mortality during 1990-2000," Bull. World Health Organ. **72**(2), 213–220 (1994).
2. N. van der Wel, D. Hava, D. Houben, D. Fluitsma, M. van Zon, J. Pierson, M. Brenner, and P. J. Peters, "M. tuberculosis and M. leprae Translocate from the Phagolysosome to the Cytosol in Myeloid Cells," Cell **129**(7), 1287–1298 (2007).
3. R. Simeone, A. Bobard, J. Lippmann, W. Bitter, L. Majlessi, R. Brosch, and J. Enninga, "Phagosomal rupture by Mycobacterium tuberculosis results in toxicity and host cell death," PLoS Pathog. **8**(2), e1002507 (2012).
4. D. Houben, C. Demangel, J. van Ingen, J. Perez, L. Baldeón, A. M. Abdallah, L. Caleechurn, D. Bottai, M. van Zon, K. de Punder, T. van der Laan, A. Kant, R. Bossers-de Vries, P. Willemsen, W. Bitter, D. van Soolingen, R. Brosch, N. van der Wel, and P. J. Peters, "ESX-1-mediated translocation to the cytosol controls virulence of mycobacteria," Cell. Microbiol. **14**(8), 1287–1298 (2012).
5. C. L. Cosma, D. R. Sherman, and L. Ramakrishnan, "The Secret Lives of the Pathogenic Mycobacteria," Annu. Rev. Microbiol. **57**(1), 641–676 (2003).
6. D. M. Tobin and L. Ramakrishnan, "Comparative pathogenesis of Mycobacterium marinum and Mycobacterium tuberculosis," Cell. Microbiol. **10**(5), 1027–1039 (2008).
7. K. Ray, A. Bobard, A. Danckaert, I. Paz-Haftel, C. Clair, S. Ehsani, C. Tang, P. Sansonetti, G. V. Tran, and J. Enninga, "Tracking the dynamic interplay between bacterial and host factors during pathogen-induced vacuole rupture in real time," Cell. Microbiol. **12**(4), 545–556 (2010).
8. C. Keller, N. Mellouk, A. Danckaert, R. Simeone, R. Brosch, J. Enninga, and A. Bobard, "Single Cell Measurements of Vacuolar Rupture Caused by Intracellular Pathogens," J. Vis. Exp. **76**(76), e50116 (2013).
9. G. Zlokarnik, P. A. Negulescu, T. E. Knapp, L. Mere, N. Burres, L. Feng, M. Whitney, K. Roemer, and R. Y. Tsien, "Quantitation of Transcription and Clonal Selection of Single Living Cells with β-Lactamase as Reporter," Science **279**(5347), 84–88 (1998).
10. LiveBLAzer™ FRET — B/G Loading Kit with CCF2-AM and CCF4-AM," *http://www.lifetechnologies.com/order/catalog/product/K1029?CID=AFLBC-425-Discovery-Sciences-K1029*.

#221113 - $15.00 USD Received 21 Aug 2014; revised 9 Oct 2014; accepted 12 Oct 2014; published 20 Oct 2014

11. W. R. Zipfel, R. M. Williams, and W. W. Webb, "Nonlinear magic: multiphoton microscopy in the biosciences," Nat. Biotechnol. **21**(11), 1369–1377 (2003).
12. M. Elangovan, H. Wallrabe, Y. Chen, R. N. Day, M. Barroso, and A. Periasamy, "Characterization of one- and two-photon excitation fluorescence resonance energy transfer microscopy," Methods **29**(1), 58–73 (2003).
13. H. Wallrabe, M. Stanley, A. Periasamy, and M. Barroso, "One- and two-photon fluorescence resonance energy transfer microscopy to establish a clustered distribution of receptor-ligand complexes in endocytic membranes," J. Biomed. Opt. **8**(3), 339–346 (2003).
14. C. Li, R. K. Pastila, C. Pitsillides, J. M. Runnels, M. Puoris'haag, D. Côté, and C. P. Lin, "Imaging leukocyte trafficking in vivo with two-photon-excited endogenous tryptophan fluorescence," Opt. Express **18**(2), 988–999 (2010), http://www.opticsinfobase.org/oe/abstract.cfm?uri=oe-18-2-988.
15. http://www.cellprofiler.org.
16. N. Otsu, "A threshold selection method from gay-level histograms," IEEE Trans. Systems, Man, and Cybernetics **9**(1), 62–66 (1979).
17. L.-Y. Gao, S. Guo, B. McLaughlin, H. Morisaki, J. N. Engel, and E. J. Brown, "A mycobacterial virulence gene cluster extending RD1 is required for cytolysis, bacterial spreading and ESAT-6 secretion," Mol. Microbiol. **53**(6), 1677–1693 (2004).
18. G. H. Patterson and D. W. Piston, "Photobleaching in Two-Photon Excitation Microscopy," Biophys. J. **78**(4), 2159–2162 (2000).
19. A. Hopt and E. Neher, "Highly Nonlinear Photodamage in Two-Photon Fluorescence Microscopy," Biophys. J. **80**(4), 2029–2036 (2001).
20. M. G. Nichols, E. E. Barth, and J. A. Nichols, "Reduction in DNA Synthesis During Two-photon Microscopy of Intrinsic Reduced Nicotinamide Adenine Dinucleotide Fluorescence," Photochem. Photobiol. **81**(2), 259–269 (2005).
21. K. König, "Cell Damage During Multi-Photon Microscopy", in Handbook of Biological Confocal Microscopy, 3rd ed., J.B. Pawley, Editor, Springer: New York. 680–689 (2006).
22. J. M. Squirrell, D. L. Wokosin, J. G. White, and B. D. Bavister, "Long-term two-photon fluorescence imaging of mammalian embryos without compromising viability," Nat. Biotechnol. **17**(8), 763–767 (1999).
23. G. W. Gordon, G. Berry, X. H. Liang, B. Levine, and B. Herman, "Quantitative fluorescence resonance energy transfer measurements using fluorescence microscopy," Biophys. J. **74**(5), 2702–2713 (1998).
24. Z. Xia and Y. Liu, "Reliable and global measurement of fluorescence resonance energy transfer using fluorescence microscopes," Biophys. J. **81**(4), 2395–2402 (2001).
25. C. Berney and G. Danuser, "FRET or no FRET: a quantitative comparison," Biophys. J. **84**(6), 3992–4010 (2003).
26. A. Zeug, A. Woehler, E. Neher, and E. G. Ponimaskin, "Quantitative intensity-based FRET approaches-a comparative snapshot," Biophys. J. **103**(9), 1821–1827 (2012).

1. Introduction

It is estimated that one-third of the world's population is latently infected with *Mycobacterium tuberculosis* (*Mtb*), and 5-10% of these latently infected individuals develop into active tuberculosis, which results in over 2 million deaths each year [1]. Transition from latency to active tuberculosis is a critical step in pathogenesis of *Mtb*. Current studies have suggested that the transition requires *Mtb* to penetrate phagosomal membrane and translocate to the cytosol of the host macrophage (termed "cytosolic translocation"), where *Mtb* replicates and spreads to other cells through cytolysis [2–4]. However, the cellular and molecular mechanisms of *Mtb* cytosolic translocation are not clear. Here, we use *Mycobacterium marinum* (*Mm*) as a surrogate model organism to study the mechanisms of mycobacterial cytosolic translocation. *Mm* causes tuberculosis-like diseases in fish, and it is also able to infect immune-competent humans where it induces formation of dermal granulomas pathologically similar to those formed in tuberculosis [5]. More importantly, *Mm* has a highly-conserved ESX-1 secretion system, which has been shown to play an essential role in cytosolic translocation of both *Mtb* and *Mm* [6]. Compared to *Mtb*, *Mm* is safer and more amenable, which will facilitate research progress.

Fluorescence resonance energy transfer (FRET) imaging has been used to monitor vacuole membrane rupture by bacteria [7, 8]. In this approach a bacterial β–lactamase-sensitive FRET reporter CCF4-AM [9], is loaded into the cell. The fluorescence donor in CCF4-AM is 7-hydroxycoumarin (blue), and the acceptor is fluorescein (green). They are linked by a cephalosporin core, which is a cleavable substrate of bacterial β–lactamase. CCF4-AM can diffuse freely across the plasma membranes and enter the cytosol. Upon entering the cell, CCF4-AM is cleaved by endogenous cytoplasmic esterases, and converts

#221113 - $15.00 USD Received 21 Aug 2014; revised 9 Oct 2014; accepted 12 Oct 2014; published 20 Oct 2014

into its negatively charged form, CCF4, an anionic molecule that is irreversibly trapped in the cytosol and excluded from endosomes and other organelles [10]. After bacteria disrupt the phagosomal membrane, bacterial β–lactamase cleaves CCF4 at the cephalosporin core, which breaks the donor and the acceptor apart and results in loss of FRET signal. By monitoring this FRET signal change, researchers have studied the spatial and temporal progress in pathogen-induced vacuole rupture. Simeone et al. observed cytosolic translocation of wild type *Mtb* strain, whereas the strains with deletion or truncation in ESX-1 secretion system remained enclosed within the phagosomal compartment [3].

In this study, we developed a two-photon excited FRET imaging method with the intention that two-photon excitation has the advantages of reduced photobleaching, photodamage and phototoxicity [11–13].

2. Two-photon FRET microscope

The schematic drawing of the two-photon FRET microscope is shown in Fig. 1. The laser source is a mode-locked Ti:Sapphire laser (Maitai HP, wavelength 690-1040 nm, 100 fs pulse width, 80 MHz repetition rate, Spectra-Physics, Santa Clara, CA). We have used 710 nm light to achieve two-photon excitation on the donor, 7-hydroxycoumarin. The laser beam is fed into a home-built video-rate (30 frames/second) x-y scanner (polygon, galvanometer). The beam passes through a dichroic beam splitter (FF665-Di02, Semrock, Rochester, NY) and is then focused onto the sample by a 60 × , NA = 1.2, water-immersion microscope objective lens (UPLSAPO60 × W, Olympus USA, Center Valley, PA). The laser power at the sample site is 10 mW. The fluorescence signal from the sample is deflected with the 665 nm long-pass dichroic mirror. A second long-pass dichoric beam splitter (FF495-Di03, Semrock, Rochester, NY) is used to split the blue and green/red fluorescence signal. The blue signal is deflected by the second dichroic beam splitter, and then is transmitted through a 417-477 nm band-pass filter (FF02-447/60, Semrock, Rochester, NY), and finally is detected by a photomultiplier tube (PMT) (R10699, Hamamatsu, Bridgewater, NJ). A third long-pass dichroic beam splitter (FF580FDi01, Semrock, Rochester, NY) is used to split the green and red fluorescence signal. The green signal is transmitted through a 500-550 nm band-pass filter (FF03-525/50, Semrock, Rochester, NY), and finally is detected by a photomultiplier tube (PMT) (R10699, Hamamatsu, Bridgewater, NJ). The red signal is transmitted through a 570-616 nm band-pass filter (FF01-593/46, Semrock, Rochester, NY), and finally is detected by a photomultiplier tube (PMT) (R3896, Hamamatsu, Bridgewater, NJ). The outputs of these three PMTs are fed into red/green/blue channels of a frame grabber (Solios eA/XA, Matrox, Quebec, Canada) installed on a computer. Two-dimensional images in x-y plane are acquired through a home-built software program. Each frame has 500 × 500 pixels. The imaging speed is 30 frames/sec and each final static image is an average of 50 frames. Details of this microscope design can be found in reference [14].

#221113 - $15.00 USD Received 21 Aug 2014; revised 9 Oct 2014; accepted 12 Oct 2014; published 20 Oct 2014

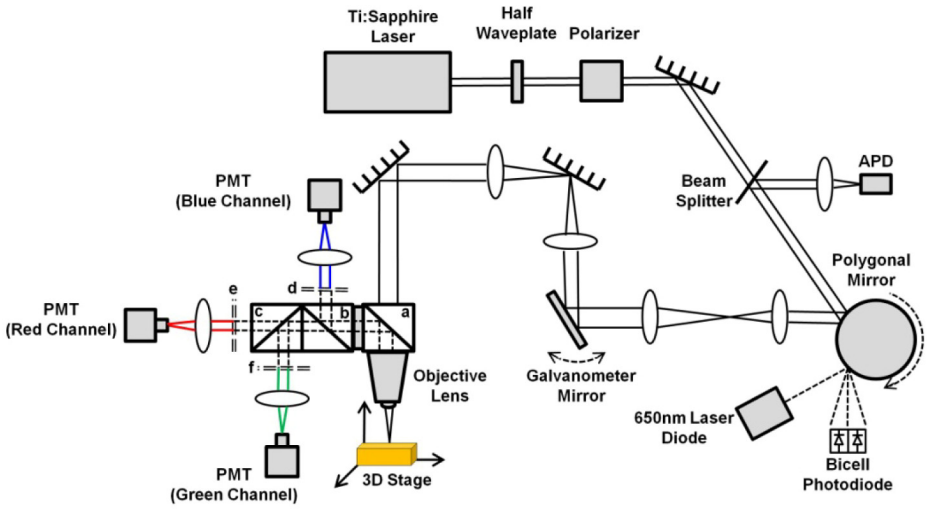

Fig. 1. Two-photon FRET microscope setup (a, b, & c: dichroic beam splitters; d, e, & f: band-pass filters).

3. Image Processing

The images acquired with our two-photon microscope were saved as 24-bit RGB TIFF files. Each of them displays 8-bit (0-255) intensity values in the red, green and blue channels respectively. They were quantitatively analyzed using the CellProfiler software [15]. A pipeline was created in order to identify cells properly and calculate the ratio of the respective mean intensity in the blue and green channels per individual cell. The following steps are used to construct a pipeline to process large amount of images: image pre-processing (Step 1), cell identification (Step 2), measurement (Step 3), calculation (Step 4), image post-processing (Step 5), and result output (Step 6).

Step 1: RGB color images (Fig. 2(a)) were converted to grayscale images by splitting the three channels into three individual grayscale images in R, G, and B respectively (Fig. 2(b)-2(d)). The green and blue channel images (Fig. 2(c) and 2(d)) are used for cell identification in Step 2; the red channel images only indicate the bacteria protein distribution.

Step 2: Each image was smoothed with a Gaussian filter in order to remove high frequency noise. Using the images (Fig. 2(c) and 2(d)) generated in Step 1, a global threshold strategy, Otsu method [16], was used to classify pixel intensities as foreground (cell) or background. This method calculates the threshold separating the two classes of pixels based on splitting the image into three classes: foreground, mid-level, and background. The mid-level intensity class was also assigned to the foreground. Cells were further identified based on diameters in the range of 10 to 80 pixels (6.4 to 51.2 μm). Cells with size outside this range were discarded. Similarly, cells located on the border of the images were not taken into account to avoid measurements from a portion of an object. The identified cells are displayed as binary cells in Fig. 2(e) which are represented with colorful patches for better visualization. Cell boundaries are demarcated with white lines as shown in Fig. 2(f).

Step 3: The average pixel intensity in G and B respectively (Fig. 2(c) and 2(d)) was measured within each cell identified in Step 2. These measurements were converted from CellProfiler default scale (0 to 1) to grayscale (0 to 255). Cells with an average pixel intensity below or equal to the background average pixel intensity were discarded from the following analyses.

Step 4: The ratio of mean blue intensity over mean green intensity was calculated for each cell based on the measurements from Step 3.

#221113 - $15.00 USD Received 21 Aug 2014; revised 9 Oct 2014; accepted 12 Oct 2014; published 20 Oct 2014

Step 5: The ratios calculated in Step 4 were displayed on top of each cell in the grayscale green channel image (Fig. 2(g)).

Step 6: RGB color images displaying cell outlines and ratios from Steps 4 were saved as TIF files. The grayscale mean intensities in G and B generated in Step 3 together with the ratios from Step 4 were exported as text files.

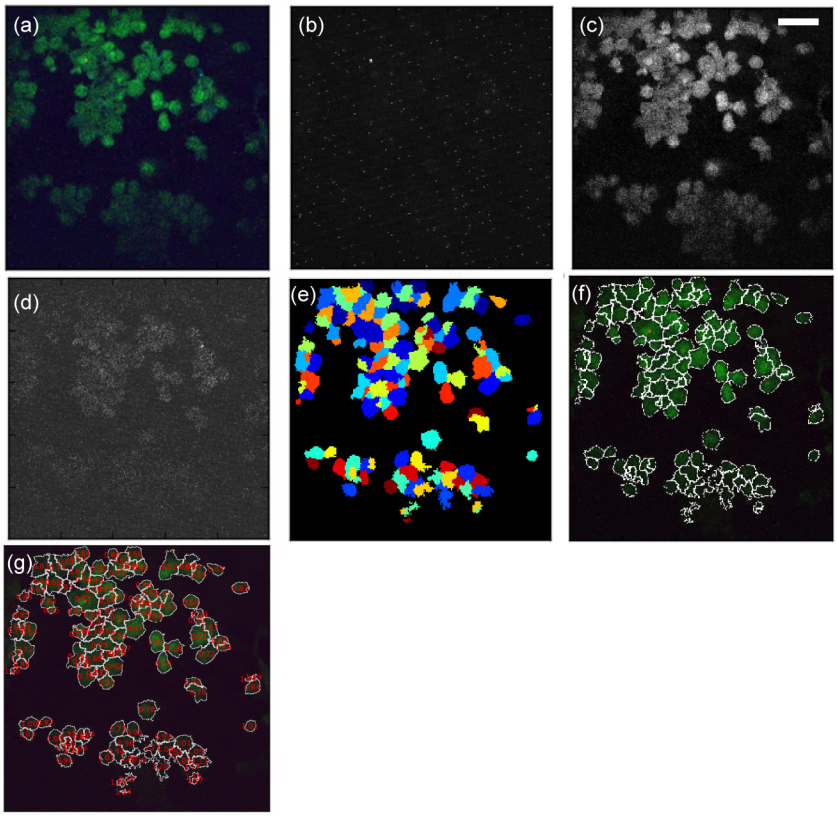

Fig. 2. Image processing and cell identification. (a) Original RGB image. (b) Grayscale image from red channel. (c) Grayscale image from green channel. (d) Grayscale image from blue channel. (e) Binary image with identified cells. (f) Cells with demarcated boundaries (g) RGB image with calculated B/G ratio displayed. (bar: 50 μm)

4. Cell Culture Preparation and Infection

The following flow chart (Fig. 3) illustrates the overview of the experimental procedure.

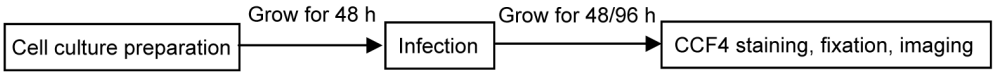

Fig. 3. Overview of the experimental procedure.

Infection

1. *Mm* strain with deletion of cfp10/esat6 (*Mm*Δc10/e6) was generated as previously described with modifications [17]. Deletion of cfp10/e6 was confirmed by PCR and western blotting analyses.
2. *To detect mycobacteria cells directly, Mm, Mm*Δc10/e6, and *Ms* cells were transformed with plasmid pMSP12::mCherry for constitutive expression of the red fluorescent protein mCherry. Transformants were selected on solid 7H10 agar

#221113 - $15.00 USD Received 21 Aug 2014; revised 9 Oct 2014; accepted 12 Oct 2014; published 20 Oct 2014

medium supplemented with 30 μg/ml kanamycin. Single colonies were picked and grown to late-log phase (OD_{600} = 1.5-1.9) in liquid 7H9 medium supplemented with 10% ADC and 0.05% Tween-80 at 30 °C. The mycobacterial cells were harvested, washed, re-suspended in PBS and then passed through a 27-gauge syringe. Single-cell bacteria were obtained by passing through a 5-μm filter (Millipore). Bacterial concentration was determined by counting cells under a fluorescence microscope.

3. RAW 267.4 mouse macrophage cells (60% confluence) were infected with *Mm* or *Ms* at an MOI of 10 in EM medium (25 mM HEPES at pH7.3, 120 mM NaCl, 7 mM KCl, 1.8 mM $CaCl_2$, 0.8 mM $MgCl_2$, 5 mM glucose). After 2 h of incubation at 32 °C, the medium was removed and the cells were washed 3 times to remove extracellular bacteria, which was followed by addition of fresh EM medium containing HEPES and 10% FBS. At 48 or 96 h post-infection, CCF4-AM FRET assays were performed as described below.

CCF4-AM FRET Assay

The assay was performed by following the product manual (Invitrogen K1095) with subtle modifications:

1. Preparation of Solution A: Add 182 (912/5) μl of DMSO to dissolve 200 μg CCF4-AM. Aliquot the solution into 20 μl/tube, and store the aliquots at –20 °C, desiccated and protected from light. Before each use, allow the frozen stock solution to thaw at room temperature and remove the desired amount of reagent. To reduce moisture uptake, recap the vial immediately after each use and return it to the desiccator in the –20 °C freezer. **Note:** Stored under these conditions, Solution A is stable for at least three months. Once thawed, Solution A may appear slightly yellow. This color change does not affect the quality or function of the product.

2. Preparation of 6 × CCF4-AM substrate loading solution

    1). Add 3 μl of Solution A to 30 μl of Solution B (100 mg/ml Pluronic®-F127 surfactant in DMSO and 0.1% acetic acid) and vortex.

    2). Add 467 μl of Solution C (24% w/w PEG 400, 18% TR-40 by volume in water) to the combined Solution A and B and vortex. **Note:** Under typical laboratory conditions, 6 × CCF4-AM substrate loading solution is stable for up to 12 hours.

3. Loading cells with substrate

    1). Add 6 × CCF4-AM substrate loading solution to cells (60-80% confluence is the best) to achieve 1 × final concentration (*e.g.,* add 20 μl of 6 × CCF4-AM substrate loading solution to 100 μl of cells in buffer).

    We made 500 μl of 6 × CCF4-AM substrate loading solution, mixed it with 2.5 ml of EM buffer. Then we added 250 μl of this mixed solution to each well.

    2). Cover the plate to protect it from light and evaporation.

    3). Incubate at room temperature for 120 minutes.

    4). Cells are washed by PBS and fixed with fresh 4% paraformaldehyde for 30 min at room temperature in the dark.

    5). Cells are washed with PBS again before performing fluorescence imaging.

#221113 - $15.00 USD Received 21 Aug 2014; revised 9 Oct 2014; accepted 12 Oct 2014; published 20 Oct 2014

5. Results

Cellular Autofluorescence and CCF-4 Fluorescence Background

Cellular autofluorescence contributes to the background in FRET measurement. Therefore, the spare cells, which went through the same cell culture processes in Section 4 but without bacteria infection and CCF4-AM staining, were imaged under the two-photon microscope. The blue, green, and red fluorescence images were shown in Fig. 4(a), 4(b), and 4(c) respectively. Both channels showed little fluorescent intensity. The quantitative measurement gave cellular background intensity around 30 in blue and green channels on a scale of 0-255 (8-bit A/D conversion of the PMT signal). And the cellular background intensity is around 40 in red channel. Cellular stress and apoptosis could possibly induce autofluorescence change. Therefore, we performed a control experiment to check cellular autofluorescence after pathogenic *Mm* infection (Fig. 4(d)-4(f)). Mouse macrophages were infected by the pathogenic *Mm* without CCF4-AM staining, and went through the same cell culture processes as the cells stained with CCF4-AM. The overall autofluorescence background for the infected cells (Fig. 4(d)-4(f)) had a slight increase compared with the uninfected cells (Fig. 4(a)-4(c)). This increase is uniform among all R, G, and B channels. Hence, the histogram of quantified B/G ratio is not changed as shown in Fig. 4(g). The bright red fluorescent patterns in Fig. 4(f) are from mCherry in bacteria, which is discussed in details later.

#221113 - $15.00 USD Received 21 Aug 2014; revised 9 Oct 2014; accepted 12 Oct 2014; published 20 Oct 2014

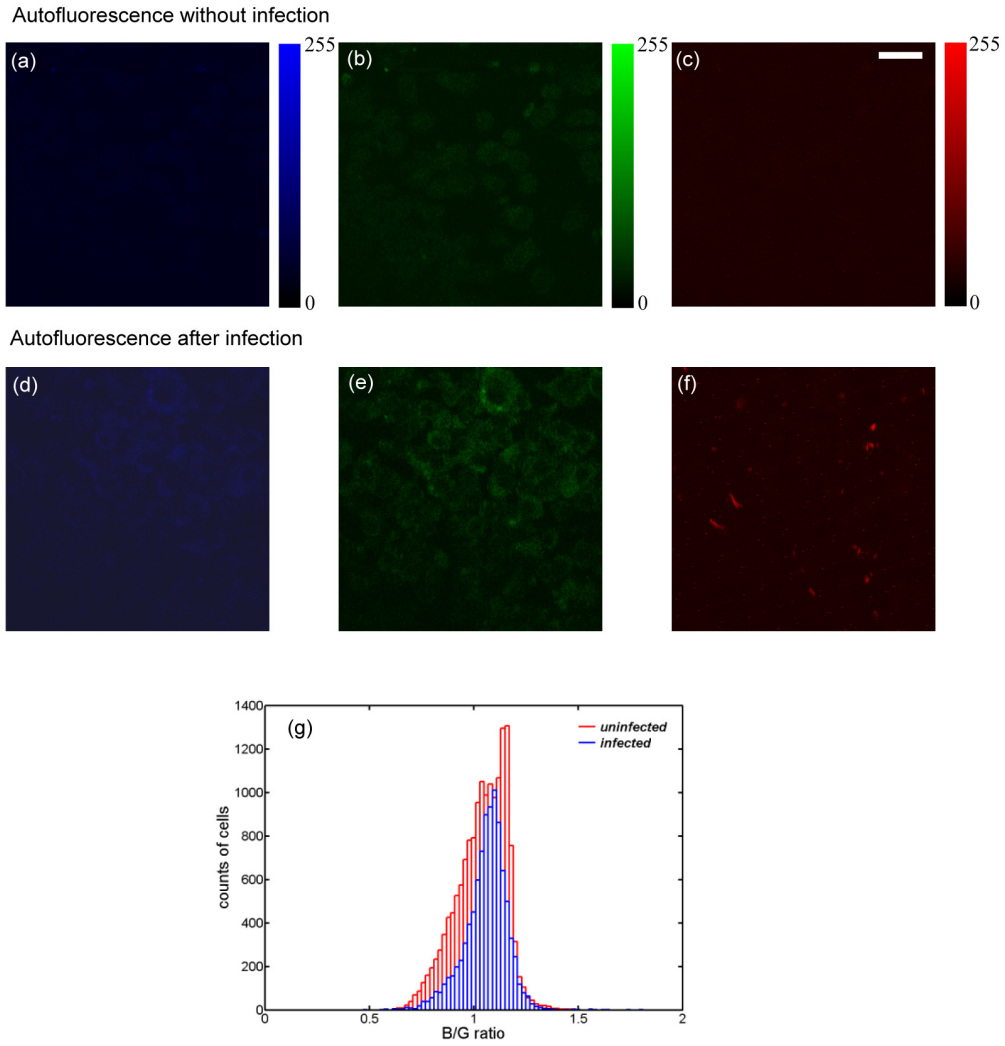

Fig. 4. Cellular autofluorescence backgrounds are minimal in blue (a) & (d), green (b) & (d), and red (c) & (f) channels from the uninfected or the *Mm*-infected cells. (g) Histograms of blue/green ratio for the uninfected (red) and *Mm*-infected cells (blue) at 96 h post-infection. The total counted *Mm*-infected cells are 9430, and the total counted uninfected cells are 16010. (bar: 20 μm)

Next, after CCF4-AM was loaded into the cells, the fluorescence signal was checked as shown in Fig. 5. The blue channel (Fig. 5(a)) showed a background similar to cellular autofluorescence. While the green channel (Fig. 5(b)) had a significant increase in intensity (typically over 100) compared with cellular autofluorescence (30-40). This indicates that CCF4-AM had been absorbed by macrophages and FRET was processed efficiently with the blue fluorescence being quenched.

#221113 - $15.00 USD Received 21 Aug 2014; revised 9 Oct 2014; accepted 12 Oct 2014; published 20 Oct 2014

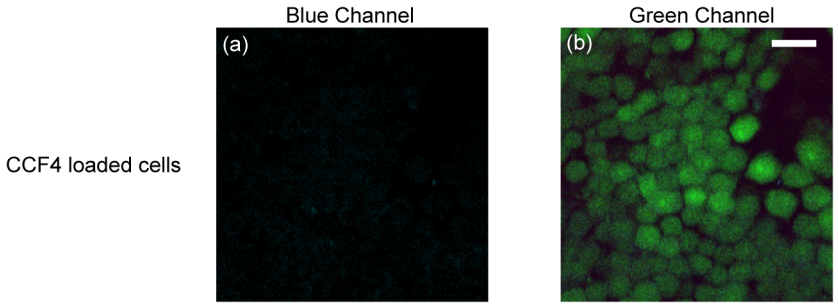

Fig. 5. CCF4 fluorescence background of the macrophages shows that the blue intensity is on the same level of cellular autofluorescence (a), while green intensity is much higher (b), indicating efficient loading of CCF4-AM into cells. (bar: 20 μm)

FRET Imaging of Mm- vs. Ms-infected Macrophages

To observe the loss of FRET signal after *mycobacteria* rupture the phagosomal membrane, RAW 267.4 macrophages were infected with *Mm*. As a control, the macrophages were also infected by *Mycobacterium smegmatis* (*Ms*), a non-pathogenic mycobacterial species that is not able to rupture the phagosome membranes. At 96 h post-infection, the images of the donor (blue) and acceptor (green) fluorescence were taken and shown in Fig. 6. Some of the *Mm*-infected macrophages showed significantly stronger blue florescence (Fig. 6(a) and 6(d)) than the *Ms*-infected cells (Fig. 6(b) and 6(e)). We also used the red channel to detect directly mycobacterial cells expressing the red fluorescent mCherry protein. As expected, the *Mm*-infected cells image (Fig. 6(j)) showed more red fluorescence than the *Ms*-infected cells image (Fig. 6(k)). More interestingly, the red fluorescence pattern from the *Mm*-infected cells showed patches (possible clusters of *Mm* bacteria), while there was dotty red fluorescence pattern from the *Ms*-infected cells. By correlating these red fluorescence images with the corresponding green fluorescence images, we found that there were more *Mm*-patches in the extracellular space (average 16 patches out of 5 randomly selected images) than the *Ms*-dots (average 8 dots out of 5 randomly selected images). This clearly indicated that *Mm* gained access to the cytosol and replicated, while majority of *Ms* were contained within phagosomes. We noticed that the blue fluorescence intensity from the *Ms*-infected cells was slightly higher than that from cellular autofluorescence, which could possibly be due to bacteria-induced apoptosis.

To further confirm the result, we infected the macrophages with the *Mm* strain whose cfp10/esat6 genes were knocked out, termed *Mm*Δc10/e6. It has been shown that deletion of cfp10/esat6 abolished the ability of *Mm* to rupture phagosome membrane and translocate to the cytosol [3]. As expected, the macrophages infected with *Mm*Δc10/e6 show similar blue, green and red fluorescence (Fig. 6(f), 6(i), and 6(l)) as the *Ms*-infected cells. This result is consistent with the current studies that the ESX-1 secretion system, including cfp10/esat6, plays an essential role of controlling cytosolic translocation of *M*m.

#221113 - $15.00 USD Received 21 Aug 2014; revised 9 Oct 2014; accepted 12 Oct 2014; published 20 Oct 2014

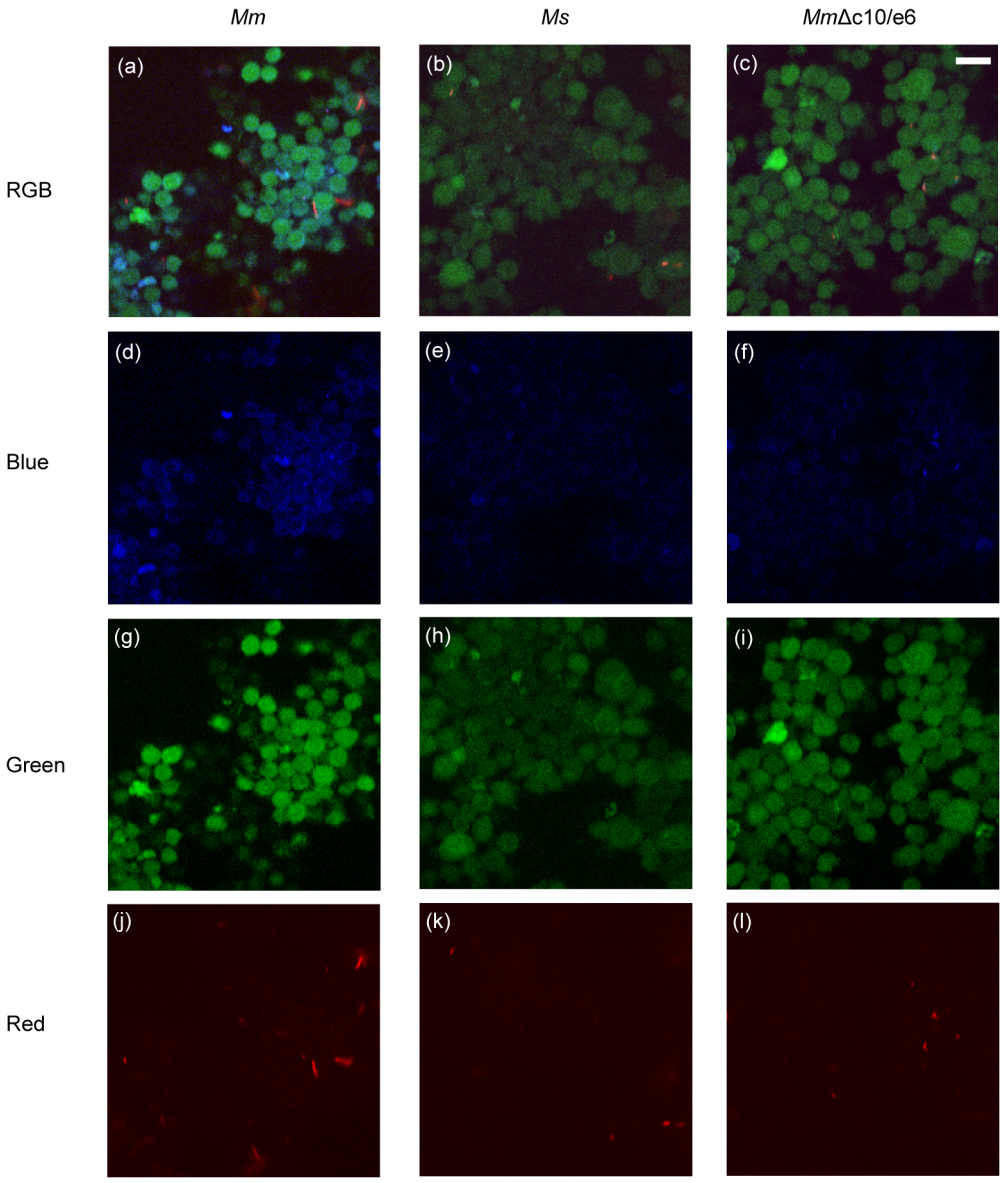

Fig. 6. At 96 h post-infection, the cells infected with *Mm* show higher blue (d) and red (j) intensity than the cells infected with *Ms* ((e)-(k)), and the cells infected with *Mm*Δc10/e6 ((f)-(l)) respectively. (bar: 20 µm)

To further quantify the difference between *Mm*- and *Ms*-infected cells, we used CellProfiler to identify cells, demarcate cell boundaries and calculate the mean intensity values in both blue and green fluorescence channels. Figure 7(a) shows the typical histograms of blue/green ratio for the *Mm*- and *Ms*-infected cells at 48 h post-infection, respectively. The number of cells analyzed for each type is more than 3000. Both histograms are similar with a blue/green ratio peak at about 1 with full width at half maximum (FWHM) about 0.35. The histogram of the *Mm*-infected cells at 96 h post-infection (Fig. 7(b)) showed an extra peak (black arrow) at higher blue/green fluorescence intensity level (~1.25) other than the main peak (~0.85), indicating FRET process was quenched, which was due to bacteria rupturing the membrane of the phagosome. The FWHM of the main peak is about 0.5. We repeatedly

#221113 - $15.00 USD Received 21 Aug 2014; revised 9 Oct 2014; accepted 12 Oct 2014; published 20 Oct 2014

observed higher counts of red fluorescence patches from the *Mm*-infected cells than the *Ms*-infected cells, indicating more *Mm* translocated into the cytosol and replicated. Comparing the 48 h and 96 h histograms, at 96 h post-infection *Mm* achieved higher incidents of cytosolic translocation than that at 48 h post-infection, while *Ms* had no significant change. One discrepancy between the histograms at different time points is not only the main peak shifts by 0.2, but also the FWHM changes by 0.15 for both the *Mm*- and *Ms*-infected cells. This could possibly be due to the precise control of the cell culture, and variation of FRET kit labeling process, which could lead to different green fluorescence backgrounds in cells. Further investigation is needed to apply this method on quantitative time-course study. With the same cell culture and labeling processes, histograms of both the *Mm* and *Ms*-infected cells showed similar main peaks and FWHMs. At 96 h post-infection the histogram of the *Mm*Δc10/e6-infected cells (green plot in Fig. 7(c)) is quite similar to that of the *Ms*-infected cells (blue plot in Fig. 7(b)). This quantitative analysis confirmed that wild-type *Mm* achieved cytosolic translocation, while *Ms* and *Mm*Δc10/e6 did not have such capability.

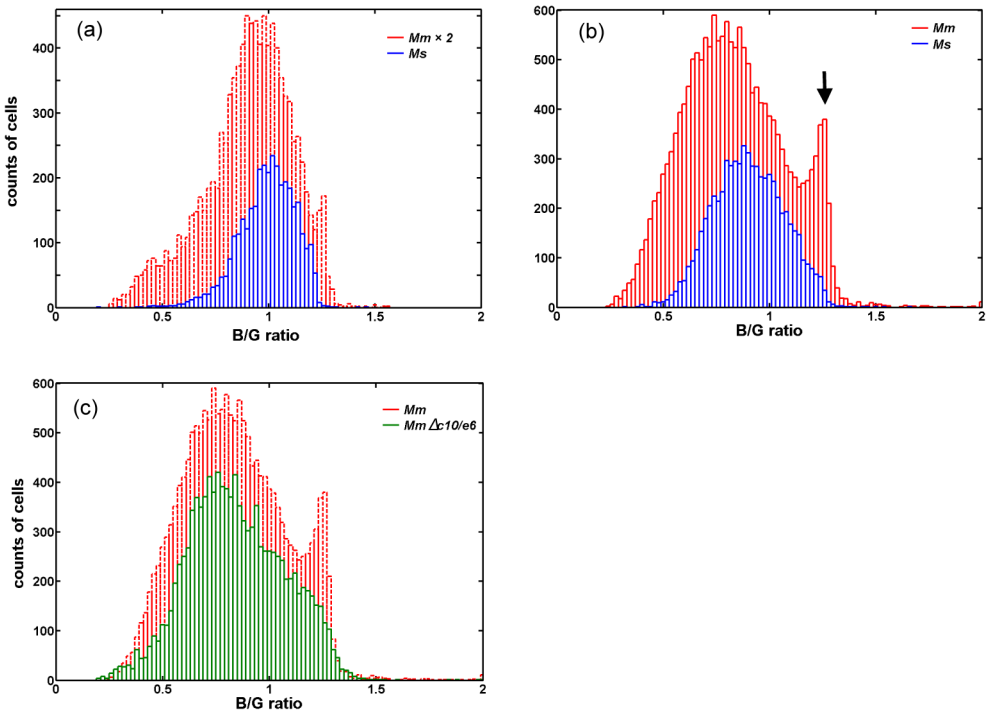

Fig. 7. Quantification of blue vs. green fluorescence intensity from cells infected with *Mm*, *Ms* and *Mm*Δc10/e6, respectively. (a) Histograms of blue/green ratio for the *Mm*- and *Ms*-infected cells at 48 h post-infection. The histogram of the *Mm*-infected cells is enlarged by 2 times. Total counted *Mm*-infected cells are 5141, and total counted *Ms*-infected cells are 3498. (b) Histograms of blue/green ratio for the *Mm*- and *Ms*-infected cells at 96 h post-infection. Total counted *Mm*-infected cells are 17593, and total counted *Ms*-infected cells are 6664. (c) Histograms of blue/green ratio for the *Mm*- and *Mm*Δc10/e6-infected cells at 96 h post-infection. Total counted *Mm*-infected cells are 17593, and total counted *Mm*Δc10/e6-infected cells are 11294.

6. Discussion

In this study, we have demonstrated using two-photon FRET imaging microscopy to quantify cytosolic translocation of mycobacteria in macrophages. The result has shown that the pathogenic bacteria *Mm,* but not the non-pathogenic *Ms,* induced a significant loss of the FRET signal, indicating that *Mm*, but not *Ms*, translocated into the cytosol, where bacterial β–

#221113 - $15.00 USD Received 21 Aug 2014; revised 9 Oct 2014; accepted 12 Oct 2014; published 20 Oct 2014

lactamase cleaved the FRET pair in CCF4. Consistent with the loss of FRET signal, the *Mm*-infected macrophages showed more red fluorescence (mCherry) than the *Ms*-infected macrophages, indicating that more *Mm* got access to the cytosol and replicated. We also noticed that intentional, prolonged exposure to 710 nm excitation pulses at the power level used here for imaging over 10 minutes did not cause any appreciable photobleaching to the cells. Two-photon microscopy can induce undesired damages due to highly nonlinear effects and even optical breakdown phenomena under certain conditions [18–20]. Under such circumstances, it requires careful control of experimental conditions, such as laser wavelength, power and illumination time, to avoid undesired photodamage. It is generally recognized that compared with confocal microscopy, two-photon microscopy has minimal photobleaching and photodamage due to the fact that two-photon excitation only happens within the focal point of sub-femtolitre volume and the excitation wavelength are in the near infrared region [21]. In a developmental biology study, live mammalian embryos were exposed for 24 hours under a two-photon microscope without measureable impact on embryo development. On the contrary, confocal microscopy imaging induced damage to embryos [22]. Hence, two-photon microscopy has the advantage of less photodamage over confocal microscopy on imaging live cells and animal imaging.

Precise measurement of the FRET efficiency requires detailed studies to minimize the potential problems, such as cross talks between FRET channels, and to optimize the concentrations of donor and acceptor molecules. By measuring the spectrum of each FRET channel, several groups have developed algorithms to quantify the FRET efficiency [23–25]. Fluorescence life time measurement can also provide extra information for better quantification of FRET efficiency [26]. Further FRET measurement using the developed method on various *Mm* mutants or *Mtb* mutants with deficiency in cytosolic translocation will reveal the specific molecular roles, and help to better understand host-*Mtb* interactions. This study has provided a novel quantitative approach for analysis of mycobacterial cytosolic translocation, which is potentially applicable to study of other bacterial pathogens in cells or in live animals.

Acknowledgment

This study was supported by College of Science Multidisciplinary Research Award Program (MRAP) at the University of Texas at El Paso to CL, JS, HO, and CX. We would like to thank Dr. Bin Cao for his help on setting up the microscope.

#221113 - $15.00 USD Received 21 Aug 2014; revised 9 Oct 2014; accepted 12 Oct 2014; published 20 Oct 2014